Initial Results from a GIS-based Unsupervised Classification Study of the Martian Surface

Eriita Jones[1,2,3], Franklin Mills[3,4], Bruce Doran[3], Graziella Caprarelli[5] and Jonathan Clarke[2]

[1] *Research School of Astronomy and Astrophysics, Planetary Sciences Institute, Mount Stromlo Observatory, Australian National University, Cotter Road, Weston ACT, 2611.*
[2] *Mars Society Australia Inc.*
[3] *The Fenner School of Environment and Society, Building 48, Australian National University, Canberra ACT, 0200.*
[4] *Research School of Physics and Engineering, Mills Road, Australian National University, Canberra ACT, 0200.*
[5] *Department of Environmental Sciences, University of Technology, Sydney, PO Box 123, Broadway, NSW 2007, Australia*

Summary: Maps of thermal inertia-albedo units and thermal inertia-elevation units on Mars' surface have been generated by choosing thresholds that fit the strongest peaks in the histograms of these datasets. The units thus defined were then interpreted as distinct mixtures of materials on the surface, such as: bright fines, rock + bedrock and ice. We have conducted an initial classification of Thermal Emission Spectrometer (TES) night-time thermal inertia and TES albedo using a hard classifier. The methods used here are largely unsupervised and differ from those of previous studies. The aim of our study is to investigate what information can be obtained by utilising unsupervised classification algorithms to investigate the distribution of thermal materials on the surface of Mars. We find that unsupervised classification reveals additional structure in the clustering and spatial distribution of surface materials with moderate-low albedo and moderate-high thermal inertia. We highlight a number of regions such as Acidalia and Valles Marineris for future detailed studies of this type.

Keywords: Thermal inertia, albedo, TES, unsupervised algorithm, clusters, ISODATA, maximum likelihood.

Introduction

Mapping of remotely measured physical parameters on planetary surfaces provides insights into the nature of the surface materials and near-surface geology. Thermal inertia and albedo are particularly useful, because these physical parameters can be acquired easily by remote observation from repeated fly overs and for long periods of time. Putzig et al. (2005) extended the work done by Mellon et al. (2000) to derive seven two-dimensional groupings of pixels, which they termed 'thermo-physical units,' from global thermal inertia and albedo datasets generated from Mars Global Surveyor (MGS) Thermal Emission Spectrometer (TES) data (Christensen et al., 2001a). These authors mapped the spatial distribution of the thermo-physical units, which they interpreted as mixtures in various proportions of three principal end-members: dust, bedrock and ice. Putzig et al.'s (2005) map was biased towards the most distinctive thermal inertia and albedo information as their method involved choosing thresholds to encompass distinctive peaks in the histograms of the data. The aim of our study is to identify whether different or additional surface features of Mars could be identified through a

less deterministic method by applying an unsupervised classification algorithm to the data.

Thermal inertia is an indicator of the ability of a material to conduct and store heat and hence it parameterises the diurnal temperature profile of surface materials (Mellon & Jakosky, 1993). Ideally, thermal inertia is derived from observations of thermal emission at multiple times of day. However, this is often not possible for spacecraft data and leads to reduced spatial resolution. Thermal inertia can also be derived from single-time observations of surface thermal emission by comparing the observations with a subsurface heat conduction model that has a surface boundary condition given by:

$$(1) \qquad \frac{S}{R^2}(1-A)\cos(i) + F_{IR} + L\frac{\partial m}{\partial t} + I\sqrt{\pi/P}\frac{\partial T}{\partial Z'}|_{Z'=0} = \varepsilon\sigma T_S^4$$

where S = solar flux, R = orbital radius of Mars, A = albedo of surface, i = the solar incidence angle, F_{IR} = thermal radiation from the atmosphere received at the surface, L = latent heat of sublimation of CO_2 (572893.8 J/kg); m = mass of CO_2 frost, I = thermal inertia, P = diurnal period, T = temperature, Z' = depth below the surface normalized to the thermal skin depth, ε = emissivity of the soil surface, σ = the Stefan Boltzmann constant (5.670400×10^{-8} $Wm^{-2}K^{-4}$), T_S = surface temperature. The thermal skin depth is the depth at which temperature fluctuations within a material drop to 1/e of their surface value. The left-hand side of the equation is the summation of the input heat received at the surface and how this heat is distributed by the surface material. The right-hand side is the heat emitted by the surface. If all parameters in the heat conduction model are well constrained then thermal inertia can be estimated with good accuracy from the heat conduction model (Mellon et al., 2000; Mellon et al., 2004). Previous studies comparing thermal inertia obtained with this method to that from multiple time of day observations have found good agreement (Christensen and Malin, 1988).
For a pure material, thermal inertia is given by:

$$(2) \qquad I = \sqrt{k\rho C}$$

with thermal inertia units (tiu) of $K/m^2/K/s^{1/2}$ where k = thermal conductivity, ρ = density, C = volumetric heat capacity. Thermal inertia is most sensitive to variations in thermal conductivity, which on Mars is strongly related to both grain size and the degree of cementation of materials (Mellon at al., 2000). Density and heat capacity of materials on Mars vary by a factor of 2-3, however thermal conductivity varies by over 3 orders of magnitude (Neugebauer et al., 1971; Table 1). Fine-grained, loosely packed materials have lower conductivity and hence lower thermal inertia while larger particles, such as rocks and ices, have higher values of conductivity and thermal inertia. Materials with low thermal inertia respond quickly to temperature changes and will closely match the phase of diurnal temperature variations (Jakosky & Mellon, 2005a-b). High thermal inertia materials are slower to respond to temperature changes so their temperature profile lags behind the diurnal variations. Furthermore, the higher the thermal inertia of the material, the smaller the amplitude of its diurnal temperature variations, as the material is effectively dispersing the incident heat throughout its thermal bulk. At the spatial scale of spacecraft observations, the surface of Mars is typically a mixture of a range of materials. This complicates interpretation of apparent thermal inertia because the diurnal and seasonal apparent thermal inertia are very sensitive to the proportions of low and high thermal inertial materials within each pixel (Putzig & Mellon, 2007a,b). Furthermore, the apparent thermal inertia for a mixture differs fundamentally from that

of either pure component due to each component having a different temperature at any given time.

Albedo is the fraction of incident visible/near-IR solar radiation (0.3 – 2.9 μm) that is reflected by the surface (Christensen et al., 2001a). Bright materials have higher values of albedo and darker materials lower. For example, dark terrestrial soils have albedo ~ 0.05 compared to ~ 0.75 for fresh snow (Ahrens, 2006). As can be observed from Eqn. 1 materials with higher albedo values have a lower maximum temperature than dark materials (Mellon et al., 2000). The average albedo for Mars is ~ 0.20, ranging from 0.07 to 0.57, where an albedo value of 0.57 is similar to terrestrial bright sand, ice or old snow (Ahrens, 2006). Albedo varies strongly with the atmospheric redistribution of dust and seasonal condensation of CO_2 and H_2O (eg. Byrne et al. 2008). For example, the global dust storm in 2001 (Smith et al. 2002) brightened surface albedo values by as much as 0.1 (Putzig & Mellon, 2007) and likely induced large perturbations in day- and night-time surface temperatures (Wilson et al. 2007). Bright regions on Mars indicate fine-grained surface dust (Rogers & Bandfield, 2007; Bandfield & Smith, 2003). Dark regions correspond to mixtures of rocks, or duricrust with smaller proportions of dust and ices. Low albedo regions have been found to have strongly homogeneous mineral compositions (Rogers & Bandfield, 2007), consisting of a mixture of minimally weathered basalt (surface type 1; Bandfield & Hamilton, 2000), altered basalt (surface type 2; Karunatillake & Squyres, 2006) and hematite (Christensen et al., 2001b).

Albedo and thermal inertia are only partially independent as both are related to thermal conductivity. As shown in Eqn. 2, thermal inertia is related to thermal conductivity by a power law. Thermal conductivity is also related to particle size with larger particles typically sharing a larger surface area with their neighbours and hence having a higher bulk thermal conductivity (for grains < 1mm under conditions on Mars; Jakosky, 1986). Albedo is correlated with particle size, with surfaces composed of larger particles typically being darker (Shkuratov *et al.* 1999) due to specular reflection. Hence albedo and thermal conductivity of surface materials are generally negatively correlated. Furthermore the albedo and thermal conductivity of a given soil varies inversely with the soil moisture, with increased water within a soil lowering the albedo but raising the conductivity (Wang *et al.,* 2005). Hence on Mars, high thermal inertia materials (eg. rocks) predominantly span a lower range of albedo values than small grained, low thermal inertia materials (eg. dust, sand). A scatterplot of global thermal inertia and albedo values on Mars (see Fig. 4 of Putzig et al., 2005) reveals the complex relationship between these variables, showing a weak negative correlation between albedo and thermal inertia for values of the latter < ~ 250 tiu (grain size ~ 170 μm) and a weakly positive correlation for thermal inertia values > ~ 250 tiu.

Thermal inertia and albedo provide two partially independent constraints on the nature of surface materials, and their combined use for mapping surface features on Mars was first demonstrated by Palluconi & Kieffer (1981). Putzig et al. (2005) chose thresholds for their thermo-physical classes that isolated the strongest modes in the histograms of the two datasets (Fig. 1) The histogram of Mars' global albedo contains three strong peaks – at 0.15, 0.23 and 0.27 (binwidth of 0.01). Thermal inertia shows two strong peaks – at 55 tiu and at 225 tiu (binwidth of 5). The former is caused by dust on Mars; the latter includes contributions from a range of materials. The methodology used in Putzig et al. (2005) in defining the unit boundaries based on the histogram peaks enables a clear detection of regions that are predominantly fine-grained surface dust because they have a very high albedo and a very low thermal inertia. However the

mixtures of materials that contribute to the two peaks at lower albedo are degenerate in thermal inertia, ie., although the materials can be distinguished through their albedo they each cover a similar range in thermal inertia (eg. Units B, C, E and G in Putzig et al. 2005, Table 1). Hence it is not clear if the somewhat arbitrary thresholds chosen in the study reflect the true underlying data structure in albedo-thermal inertia space. It is for this reason that we have employed an unsupervised algorithm that iteratively groups pixels based on minimising their Euclidean separation in albedo-thermal inertia space.

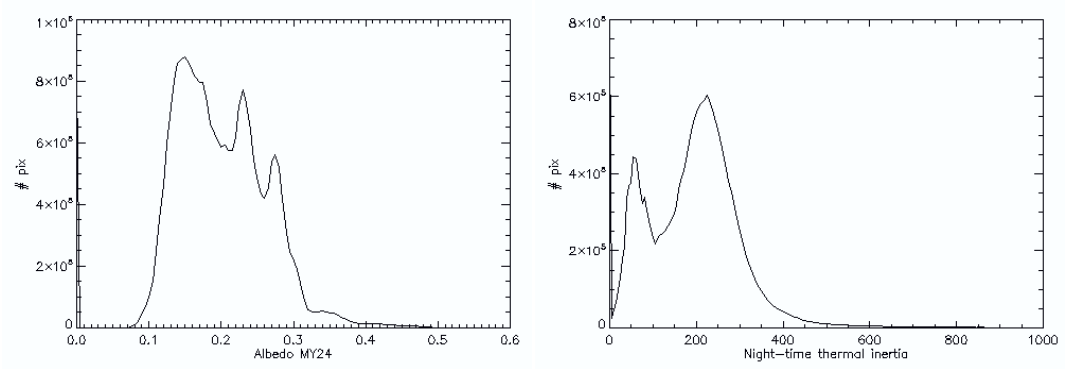

Figure 1: Histograms of the global albedo (left) and night-time thermal inertia (right) data sets. Horizontal axis has been cropped to focus on peaks. Both datasets are multi-modal and contain 2.592 x 10^7 pixels.

Unsupervised classification techniques have recently been applied to Martian Digital Terrain Models to identify topographic features such as craters and valley ridges (eg. Stepinski *et al.,* 2005, 2009a,b) however they have not been utilized to identify the distribution of thermally distinct surface materials. Mapping the thermal behavior of surface material on Mars has many interesting applications, one of which is constraining subsurface temperature profiles which can then be utilized to estimate the range of depths at which liquid water or brine could exist (eg. Jones & Lineweaver, 2010).

Methods

The technical specifications of the Mars Global Surveyor Thermal Emission Spectrometer used to collect the albedo dataset and the data from which thermal inertia is derived are described in detail in Christensen et al. (2001a). The two global datasets used in this study – Mars Year 24 (MY24) albedo and night-time thermal inertia - were obtained from http://lasp.colorado.edu/inertia/2007/albedo.html (2007 Global MGS-TES Albedo Maps) and http://lasp.colorado.edu/inertia/2007/ (2007 Global MGS-TES Thermal Inertia Maps). The MY24 data were selected because MY24 had minimal localised dust storm events (Cantor et al., 2002) and generally a lower dust optical depth (the atmosphere was more transparent) than MY25 and 26 (Tamppari et al., 2008; Smith 2004), which are also available. This means that the derived albedo values for MY24 will be more representative of the mean surface materials and less affected by scattering due to atmospheric dust. The datasets have dimensions of 7200 x 3600 pixels which correspond to a resolution of 0.05° per pixel or ~3 km². The data sets have been bilinearly interpolated between the MGS orbital tracks with real data constituting ~93% of the thermal inertia map and ~35 % of the albedo map (Putzig pers. comm.). The uncertainty in albedo values is approximately ± 0.01 (Christensen et al., 2001a) and the uncertainty associated with each derived night-time thermal inertia value is estimated

to be < 10% (Putzig & Mellon, 2005), lower than for daytime measurements (error < 17%). The TES sensing depth is on the order of several centimeters (Mellon et al., 2000), so TES provides information only on surficial levels of the crust. Data was analysed using: off-the-shelf commercial software, ArcMap 9.2, for description, mapping and visualization of the distribution of the classes; and IDL for data manipulation prior to importing into ArcMap and analysis. Classification algorithms were used to find 7 distinct clusters in the data, so that a direct comparison with the 7 clusters defined by Putzig et al. (2005) could be undertaken.

Walker *et al.* (1986) gave one of the earliest presentations of the technique of unsupervised classification by using a scatter plot of pixel values in two spectral bands to separate land cover features. Unsupervised classification is now broadly used in the interpretation of terrestrial remote sensing data (Hall et al., 1995). The technique involves using a clustering algorithm to group pixels in parameter space that have similar values within each measurement parameter (parameters are typically red and near-infrared reflectances in a terrestrial LANDSAT image but are albedo and thermal inertia in this study) without *a priori* knowledge of the surface materials present. This is often necessary with remotely sensed data of a large or complex area as the actual or optimum number of natural clusters in the data is not known and the amount of data is so vast that it must be reduced before field data can be collected to define the link between remotely sensed pixel values and surface land cover. By grouping observations and minimizing the differences between members in a group, the spatial locations that are most similar can be identified (Duda & Hart, 1973; Murray & Estivill-Castro, 2001). Once a cluster dataset has been produced, each cluster can then be interpreted as a mixture of materials on the surface with the values for each cluster used to determine some of the attributes of those surface materials (Jupp *et al.,* 1986).

There are two fundamental caveats to the technique of unsupervised classification. Firstly, the number of clusters to be found by the classification algorithm must be chosen by the user (e.g. Milligan & Cooper, 1985) and hence may not reflect the full complexity of natural patterns within the data. Secondly, there may be several acceptable clusterings of the dataset, depending upon the purposes of the application. Despite this, cluster outputs produced by unsupervised classification using the maximum likelihood decision rule applied in this study have been applied successfully in terrestrial remote sensing (e.g. Belward et al., 1990). Studies using LANDSAT-TM, MSS and ETM imagery which use field data to assess the accuracy of the unsupervised classification, report accuracies (i.e. the percentage of pixels within a cluster that have been identified as belonging to that cluster) of 60 – 90% (Miller & Yool, 2002; Sader *et al.,* 1995; Murthy *et al.,* 2003). Whilst comparable field data is not readily available for analysis of remotely sensed Mars data, the generic unsupervised classification approach and associated techniques used in terrestrial applications are transferrable.

The albedo and thermal inertia datasets were both normalized before classification by scaling the max and min to the range [0,1]. The algorithms used to generate the 7 two-dimensional clusters were ISODATA (Iterative Self-Organizing Data Analysis Technique) and Maximum Likelihood Classification (MAXLIKE) run through ArcGIS 9.2, using the calling commands ISOCLUSTER and MLCLASSIFY, respectively. ISODATA is an unsupervised training algorithm which uncovers the statistical patterns inherent in the data. It is useful when little is known about the data prior to classification. ISODATA works by examining a subset of the data (every 5th pixel in this study) to provide candidate clusters which are then fed into the clustering algorithm. These candidate

clusters are analogous to the training data that would be used in a supervised classification (for example, if the signatures of a certain type of feature in the dataset were known before classification). The user inputs the maximum number of clusters to generate (7 in this study) and then the algorithm iteratively passes through the dataset defining clusters until either the maximum number of iterations is reached (specified by user; Ball & Hall, 1965; Richards, 1986) or there is little change in clusters between iterations (Swain 1973). Pixels are determined to be similar if they have similar values in each of the n-input parameters (Tou & Gonzalez, 1974). Calculating the parameter distance using the Euclidean distance equation (Richards, 1986; p.190[1]), the ISODATA algorithm assigns pixels to a cluster if the parameter distance between the pixel and the cluster centre is less than the distance to all other cluster centers. To do this, an initial vector with a mean value for N clusters (where N is the maximum number of final clusters specified by the user) is defined so that the N initial arbitrary cluster centers are uniformly spaced along the multidimensional diagonal ensuring that the initial assignment of cluster centers is not biased to the extrema of the input data. The location of the initial cluster means is not important so long as enough iterations are allowed (500 in this study) for the clusters to become stable. On the first pass through the data, each pixel is compared with the vector and assigned to the cluster whose centre is closest in parameter distance. After the first pass through the data the cluster centers are redefined and new centers are calculated by taking the sample mean of pixels assigned to each cluster in the previous step. The process then continues iteratively. The final number of clusters can be less than N when: (a) a minimum cluster size S is specified (in this study S = 30, corresponding to 0.0001 % of the dataset) so that any clusters consisting of fewer cells will be eliminated at the end of an iteration; or, (b) clusters close in parameter space and with similar statistical values become merged during the iterative process The assignment of clusters is independent of the contiguity of the pixels in the spatial frame.

The candidate clusters provided by ISODATA are described in a signature file that provides the mean and covariance matrix for each parameter in each cluster and is used to train the classification algorithm MAXLIKE. MAXLIKE assumes that the distribution of each cluster will be multivariate normal (depending on the number of parameters in the classification, hence bivariate normal[2] in this study) so that each cluster can be characterized by the statistical parameters provided in the signature file for the corresponding training cluster. Each pixel in the dataset is then assigned to a single cluster according to the Boolean decision rule based on probabilities from the normal distributions. A pixel X belongs to the cluster S_i if the probability of X belonging to S_i is greater than the probability of X belonging to S_j, for all j≠ i'. Hence each pixel is assigned to the cluster to which it has the highest probability of being a member, irrespective ofthe actual probability of membership. It is assumed that all clusters have an equal probability of occurring. The MAXLIKE algorithm works best with a normal distribution of data (Kloer, 1994). If the histograms of the input parameters are strongly non-normal (as in this study; Fig. 1) the algorithm can overestimate χ^2 (chi-squared) classification errors (Benson & Fleishman, 1994). This problem is minimized with an increasing

[1] The parameter distance is calculated by the Euclidean distance equation: $D_j = \left(\sum_{i=1}^{dim}(x_i^2 - s_i^2)\right)^{1/2}$ where dim = the number of data dimensions (in this study, dim = 2), x = data vector, s = cluster centre vector.

[2] The bivariate normal distribution has probability density function: $P(x,y) = \frac{1}{2\pi\sigma_x\sigma_y\sqrt{1-\rho^2}} exp\left[-\frac{z}{2(1-\rho^2)}\right]$ where $z = \frac{(x-\mu_x)^2}{\sigma_x^2} + \frac{(y-\mu_y)^2}{\sigma_y^2} - \frac{2\rho(x-\mu_x)(y-\mu_y)}{\sigma_x\sigma_y}$, $\rho = \frac{v_{xy}}{\sigma_x\sigma_y}$ and μ = mean, σ = stanard deviation, v = covariance (Wackerly *et al.,* 2002; p. 268).

number of data points in the total sample and has been found to be negligible if the number of data points is > 400 (Harlow et al., 1985).

The validity of the clusters defined by MAXLIKE can be quantified through the χ^2 distribution with degrees of freedom equal to the number of input parameters (Swain & Davis, 1978; Richards, 1986). This provides a measure of the classification confidence by giving the percentage chance for each pixel that it has been assigned to the correct cluster, based on the separation distance between the pixel value and the cluster mean in the multiparameter space. Essentially, if the number of pixels in a given cluster is plotted against their parameter distance from the cluster mean this will ideally follow a χ^2 distribution (Richards, 1986 p. 174). Thus, if a threshold confidence value of 97.5% is imposed, the least likely 2.5% of pixels in the cluster (those with χ^2 values greater than 7.4 for 2 degrees of freedom) will be rejected (Wackerly et al. 2002 , p. 794). The χ^2 statistics are generally applied to independent variables. Although the covariance of the (normalized) albedo and thermal inertia datasets used in this study is non-zero (cov = 0.002), it is small compared to their individual variances (0.015 and 0.011, respectively). The MAXLIKE algorithm run through ArcMap outputs a confidence raster based on the χ^2 distribution (see Results), which provides the level of confidence with which each cell was classified. For example, cells with a value of 5 have a 95% chance of having been correctly classified. Furthermore, the presence of clear unfragmented spatial patterns in the classification map provides anecdotal evidence that the classifier is producing a reasonably accurate model (Gahegan & West, 1998).

Interpreting thermal inertia & albedo

The atmosphere of Mars is never dust free and the surface, globally, is dominated by particulate matter (Bandfield *et al.,* 2000). Understanding the thermal inertia and albedo signatures of these fines is key to interpreting the thermo-physical units. Albedo is strongly correlated with the degree of fine, bright dust coverage (Kieffer, 1973; Ruff & Christensen, 2002). Surfaces on Mars covered by fine, bright dust have an albedo > 0.25 and a low value of thermal inertia because of the low thermal conductivity of small particles. A combination of infrared spectral analysis and studies of analogue materials at Martian surface pressures showed that dust on Mars typically has diameters less than ~ 40 micrometers (Christensen, 1986) which correspond to a thermal inertia < 65 tiu (Jakosky 1986). Larger, coarse, unbonded particulates from 100 - 10^4 micrometres dominate the low albedo regions of Mars (Christensen & Moore, 1992). For grains up to ~ 1000 micrometres across (thermal inertia ~ 200) laboratory studies show that thermal conductivity increases linearly with particle size (Jakosky, 1986) and, hence, the thermal inertia generally increases with the square root of grain size. Larger particulates have a thermal inertia ~ 400 tiu (Jakosky, 1986). Thus, the combination of thermal inertia and albedo can be used to identify surfaces that are completely covered by fine-grained dust. Identifying larger darker fines (mm – cm) is more difficult, however, as both (i) their albedo is consistent with rocks and duricrust and (ii) their thermal inertia is consistent with a sub-pixel-scale mixture fine dust with high thermal inertia materials (such as rocks). Hence, intermediate values of thermal inertia do not have a unique interpretation given they can result from a range of mixtures of materials. Materials such as rock and ice are more easily identified through thermal inertia, as values above 2500 tiu can only be regions that are pure or almost pure rock or ice. Representative values drawn from laboratory, in-situ, observational, and modelling analyses for the thermal inertia of some materials on Mars are shown in Table 1.

Table 1: Representative properties of some materials on Mars (taken from Jones & Lineweaver, 2011 in prep.)

Material	Grain size (mm)	Thermal conductivity ($Wm^{-1}K^{-1}$)	Density (kgm^{-3})	Heat capacity ($Jkg^{-1}K^{-1}$)	Thermal diffusivity (m^2s^{-1})	Calculated TI (Eqn. 2)	References
Dust	<< 1 x 10^{-3} -0.1	0.001	1000	800	1.3 x 10^{-9}	28	Mellon & Phillips 2001 Jakosky 1986 Karunatillake et al. 2010
Sand	0.1 - 10	0.1	1750	800	7.1 x 10^{-8}	374	Mellon & Phillips 2001 Heldman *et al.* 2005 Murphy *et al.* 2009 Jakosky 1986
Duricrust	Highly variable; sand size particles cemented to form larger grains	0.3 (up to 2)	1750	800	2 x 10^{-7}	648	Murphy *et al.* 2009 Piqueux & Christensen 2009 Fergason et al. 2006
Icy soil	N/A	2.5	2018	1040	1.2 x 10^{-6}	2294	Mellon *et al.* 2004 Sizemore & Mellon 2006
Rock	> 40	2.5 (range generally 1.5-4.5)	2900	800	1 x 10^{-6}	2408	Clauser & Huenges, 1995 Turcotte *et al.* 2002 Sizemore & Mellon 2006 Golombek et al. 2005 Mellon & Phillips 2001
H_2O ice	N/A	3.4 (at -110 ˚C ; 2 at 0˚C)	928	1310	1.3 x 10^{-6}	2044	Clauser & Huenges 1995 Titus *et al.* 2003

Each TES pixel is of order 3 km^2, which makes it unlikely any pixel contains only one type of surface material, so each of our thermo-physical units is interpreted as a 'mixture' of materials on the surface of Mars. Our interpretation of the material components of each cluster is based on matching the albedo and thermal inertia peaks in Fig. 2 to the estimated parameters of materials on Mars shown in Table 1. The main components of the mixtures of materials in each of the 7 clusters are given in Table 2.

As expected, the main source of uncertainty in interpreting the results of the calculations is the degeneracy of the thermal inertia-albedo data (see Introduction). For example, the peak in thermal inertia at ~ 250 tiu (Clusters 1-4 in Fig. 2) is consistent with either pure coarse- grained unconsolidated particles, such as sand, or a mixture of duricrust (~600 tiu), dust (~50 tiu) and sand (~ 300 tiu). An albedo below ~ 0.2 implies the absence of significant amounts of fine, bright dust and hence the thermal inertia is interpreted as a weighted average of the amount of duricrust and sand where the weights vary.

Results

The seven thermo-physical units defined in this study are mapped in Fig. 3 and details are given in Table 2. A pattern of global 'enveloping' can be seen in the spatial occurrence of the 7 clusters, mirrored on either side of the Equator (Fig. 3). This corresponds to a decrease in albedo with increasing distance from the Equator through the sequence of clusters 5 ⟶ 4 ⟶ 3 ⟶ 2 ⟶ 1. The mean thermal inertia also increases through this sequence - with the exception of Cluster 3 – and the values indicate that the fraction of bright dust and fine grained sand is decreasing with progression through the cluster sequence. However, Cluster 3 is an exception to this as it has a thermal inertia peak corresponding to fine, unconsolidated material, associated with a decreased albedo relative to Cluster 4. This may be a detection of dark fines. Cluster 3 is also present near the South Pole where it corresponds to Putzig et al.'s Class D (light blue) which was interpreted by these authors as 'dark dust'. If this interpretation is correct, it covers an extensive area of the surface of Mars, predominantly in the southern polar terrain but also infilling Hellas Basin, Promethei Terra and the albedo feature west of Elysium.

The map in Fig. 2 has associated error maps provided in Fig. 3. These maps indicate which regions were most likely to have been classified accurately by the unsupervised algorithm. 58% of pixels in Fig. 2 are most likely classified correctly, as they fall within the 50% confidence interval (Fig. 3). The 50% confidence interval contains pixels from each of the seven thermo-physical units indicating that that the general surface locations in which these clusters occur is fairly well constrained. The core spatial patterns of each cluster are maintained in both the 50% and 75% confidence interval maps. The most accurate pixels, classified with $>$ 95% confidence, comprise 15% of the map. These pixels are located primarily equatorwards of $\pm$ 70˚ and very few of them belong to cluster 6.

Table 2: Some details of the 7 thermo-physical units from this study in the form: mean, standard deviation.

Cluster	Thermal inertia (tiu)	Albedo (%)	Interpretation
1	260, 70	13, 1	Duricrust, rocks, sand
2	230, 70	16, 1	Duricrust, sand
3	180, 80	20, 1	Duricrust, sand, dark fines
4	200, 80	24, 1	Duricrust, sand, dust
5	80, 50	28, 2	Dust
6	410, 340	35, 6	Ice
7	3670, 920	30, 7	Ice, rocks

Both the thermo-physical map of Putzig *et al.* (2005) and the map produced in this study closely match previous determinations of the global spatial pattern of Mars' fine, bright dust cover (Ruff & Christensen, 2002, Bandfield *et al.,* 2000). There are broad similarities between our map and that of Putzig *et al.* (2005), particularly in the equatorial regions of Mars where small unconsolidated particles dominate. The spatial boundary of Cluster 5 in this study closely matches Putzig *et al.* (2005) Class A (blue) and is dominated by dust (Ruff & Christensen, 2002). The distribution of Cluster 4 is very similar to Putzig *et al.* (2005) Class C (green), although Cluster 4 appears to be always associated with Cluster 3, which was not differentiated in the Putzig *et al.* (2005) study (it was part of Class B, yellow). Other differences between the results of this work and Putzig *et al.* (2005) are that our Classes 1 and 2 are not differentiated in Putzig *et al.* (2005), as their classification incorporated them into their broad mid-latitude Class B. Our Cluster 6 occurs at the poles and incorporates high-latitude data published in Putzig and Mellon (2007; hence not included in the Putzig *et al.* (2005) map). Possible anomalously high thermal inertia values occurring at the North Pole are contained in Putzig *et al.* (2005) Class E and our Cluster 7.

In synthesis, both maps classify bright regions (eg. Tharsis, Arabia and Elysium) as being dominated by the same thermo-physical unit, which is interpreted as fine, bright dust deposits at least several centimetres thick.. The main differences occur in low albedo regions (eg. Acidalia and Sinus Meridiani), which will be investigated in follow-up studies.

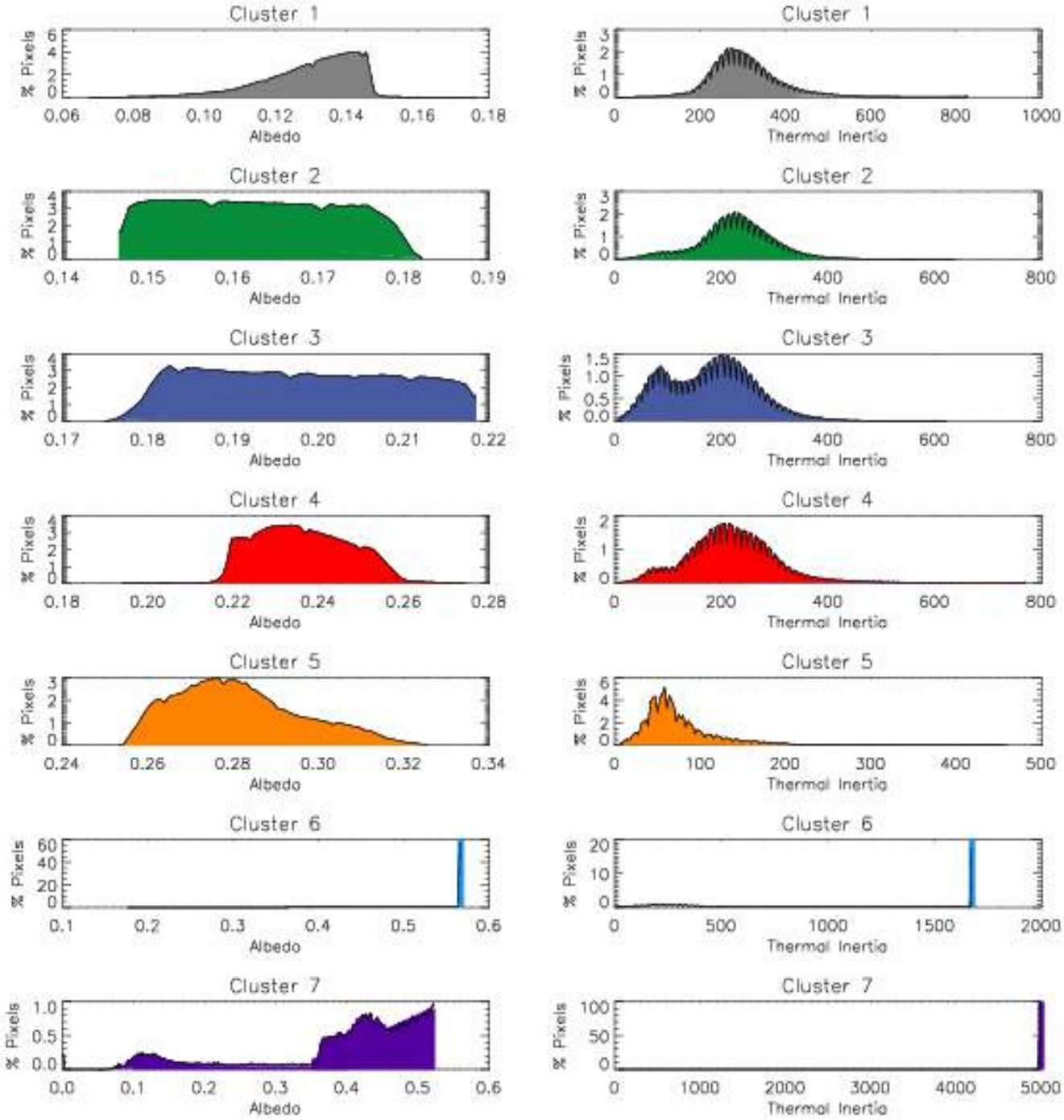

Figure 2: Histograms of albedo and thermal inertia for the 7 thermo-physical units.

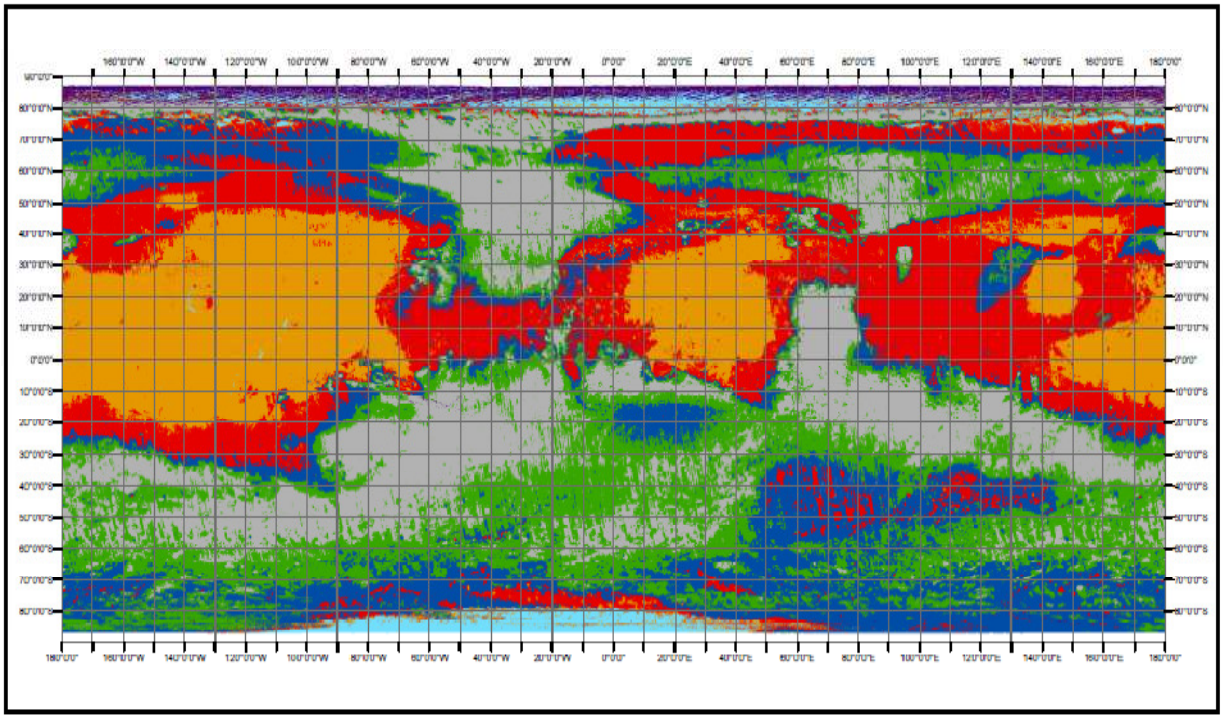

Figure 3: Unsupervised classification of TES albedo and night-time thermal inertia into seven thermo-physical units. Details of the units are given in Table 2 and histograms in Figure 2.

Conclusions

We have used albedo and night-time thermal inertia data of the surface of Mars and an unsupervised classification method to identify seven mappable thermo-physical units. Our results refine previous studies (Putzig et al., 2005; Putzig and Mellon 2007a,b) of the distribution of rock, dust and ice on the surface. We interpreted the thermo-physical units by comparing the peaks in the albedo and thermal inertia histogram of each unit to representative values of materials on Mars. Our results agree with previous studies in the equatorial region where bright fines dominate. However, we find evidence of additional structure in the distribution of surface materials at higher latitudes, particularly in areas of low albedo and moderate-high thermal inertia. Further studies will need to be undertaken to resolve the reasons for the differences and determine the nature of the surface material at high latitudes. This work significantly demonstrates that unsupervised classification can detect potentially important structure in surface materials on Mars at a higher spatial resolution than that provided in previous studies.

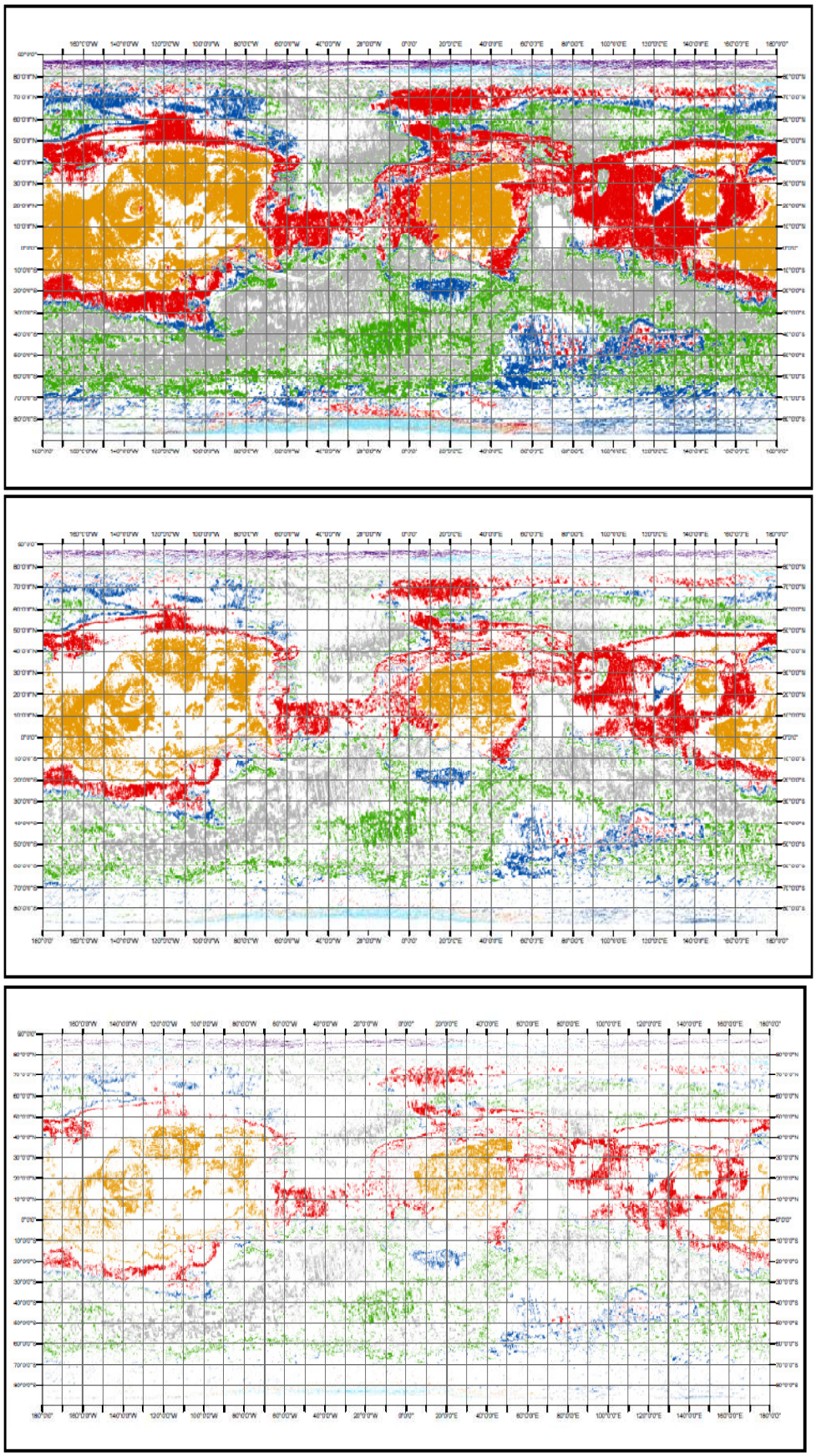

Figure 4: Classification error map at 50%, 75% and 95% confidence intervals. Pixels are either coloured to match their cluster assignment in Figure 3, or coloured white. White pixels have either a: > 50% chance of being classified into the wrong cluster (top); > 25% chance of being misclassified (middle); or > 5% chance of being misclassified (bottom; see details on χ^2 distribution in text).

Acknowledgements: ArcGIS 9.3 Online Help, Topics: "How Maximum Likelihood Classification Works" and "How Iso Cluster Works", ESRI, 2010.
ERDAS Inc., "Unsupervised Training" and "Evaluating Classification" published in ERDAS Field Guide (3rd Ed), Atlanta, 1994, pp. 240-247 and pp. 270-278 respectively.

References

1. Ahrens, C. "Meteorology Today: An Introduction To Weather, Climate, and The Environment (8th Ed.)", Cengage Learning, USA, 2007, p. 44.
2. Ball, G.H., Hall, D.J., "ISODATA, A Novel Method of Data Analysis and Pattern Classification", Stanford Research Institute, California, 1965.
3. Bandfield, J. L., Hamilton, V. E., Christensen, P.R., "A Global View of Martian Surface Compositions From MGS-TES", *Science*, Vol. 287, 2000, pp. 1626-1630.
4. Bandfield, J. and Smith, M., "Multiple Emission Angle Surface-Atmosphere Separations of Thermal Emission Spectrometer Data", *Icarus*, Vol. 161, 2003, pp. 47-65.
5. Belward, A.S., Taylor, J.C., Stuttard, M.J., et al., "An Unsupervised Approach To The Classification of Semi-Natural Vegetation From Landsat Thematic Mapper Data. A Pilot Study On Islay", *International Journal of Remote Sensing*, Vol. 11, 1990, pp. 429-445.
6. Benson, J., Fleishman, J.A., "The Robustness of Maximum Likelihood and Distribution-Free Estimators To Non-Normality In Confirmatory Factor Analysis", *Quality and Quantity,* Vol. 28, 1994, pp. 117-136.
7. Byrne, S., Zuber, M.T., Neumann, G.A., "Interannual and Seasonal Behaviour of Martian Residual Ice-Cap Albedo", *Planetary and Space Science*, Vol. 56, 2008, pp. 194-211.
8. Cantor, B.A., Malin, M., Edgett, K.S., "Multiyear Mars Orbiter Camera (MOC) Observations of Repeated Martian Weather Phenomena During The Northern Summer Season", *Journal of Geophysical Research*, Vol. 107, 2002, E001588.
9. Christensen, P.R., "Regional Dust Properties On Mars: Physical Properties, Age and History", *Journal of Geophysical Research*, Vol. 91, 1986, pp. 3533-3545.
10. Christensen, P.R., Malin, M.C., "High Resolution Thermal Imaging of Mars", *Lunar and Planetary Sciences Conference,* Vol. 19, 1988, pp. 180-181.
11. Christensen, P.R., Moore, H.J., "The Martian Surface Layer", in *Mars*, Kasting, J., Eds, 1992, pp. 686-729.
12. Christensen, P.R., Bandfield, J.L., Hamilton, V.E., and 23 others, "Mars Global Surveyor Thermal Emission Spectrometer Experiment : Investigation Description and Surface Science Results", *Journal of Geophysical Research*, Vol. 106, 2001a, pp. 23823-23871.
13. Christensen, P.R., Morris, R.V., Lane, M.D., et al., "Global Mapping of Martian Hematite Mineral Deposits: Remnants of Water-Driven Processes On Early Mars", *Journal of Geophysical Research*, Vol. 106, 2001b, pp. 23873-23885.
14. Clauser, R., Huenges, E., "Thermal Conductivity of Rocks and Minerals" in Rock Physics and Phase Relations – A Handbook and Phase Relations, Ahrens, T., Eds, American Geophysical Union, 1995, pp. 105-126..
15. Duda, R.O., Hart, P.E., "Pattern Classification and Scene Analysis", *Wiley Publishers*, New Jersey, 1973.
16. Fergason, R.L., Christensen, P.R., Bell III, J.F., et al., "Physical Properties of the Mars Exploration Rover Landing Sites As Inferred From Mini-TES-Derived Thermal Inertia", *Journal of Geophysical Research,* Vol. 111, 2006, E02S21.
17. Gahegan, M., West, G., "The Classification of Complex Geographic Datasets: An Operational Comparison of Artificial Neural Networks", *Geocomputation Conference*, 1998. Accessible at: http://www.geocomputation.org/1998/61/gc_61.htm
18. Golombek, M.P., Arvidson, R.E., Bell, J.F., and 13 others, "Assessment of Mars Exploration Rover Landing Site Predictions", *Nature,* Vol. 436, 2005, pp. 44-48.

19. Hall, F.G., Townshend, J.R., Engman, E.T., "Status of Remote Sensing Algorithms For Estimation of Land Surface State Parameters", *Remote Sensing of Environment*, Vol. 51, 1995, pp. 138-156.
20. Harlow, L., Chou, C.P., Bentler, P., "Performance of Chi-Square Statistic With ML, ADF, and Elliptical Estimators for Covariance Structures", *Annual Meeting of the Psychometric Society*, Toronto, Canada, 1986.
21. Heldman, J., Toon, O., Pollard, W., et al., "Formation of Martian Gullies By The Action of Liquid Water Flowing Under Current Martian Environmental Conditions", *Journal of Geophysical Research*, Vol. 110, 2005, E05004.
22. Jakosky, B. M., "On the Thermal Properties of Martian Fines", *Icarus*, Vol. 66, 1986, pp. 117-124.
23. Jakosky, B.M., Mellon, M.T., Varnes, S., et al., "Low-Latitude Neutron Distribution: Possible Remnant Near-Surface Water Ice and A Mechanism For Its Recent Emplacement", *Icarus*, Vol. 175, 2005a, pp. 58-67.
24. Jakosky, B.M., Mellon, M.T. , Varnes, S., et al., "Erratum to Low-Latitude Neutron Distribution: Possible Remnant Near-Surface Water Ice and A Mechanism for Its Recent Emplacement", *Icarus*, Vol. 175, 2005b, pp. 58-67.
25. Jones, E.G., Lineweaver, C.H., "To What Extent Does Life 'Follow the Water'?", *Astrobiology*, Vol. 10, 2010, pp. 349-361.
26. Jones, E.G., Lineweaver, C.H., "Phase diagram of the Potential Martian Biosphere", 2011, in preparation.
27. Jupp, D.L., Walker, J., Penridge, L.K., "Interpretation of Vegetation Structure In Landsat MSS Imagery: A Case Study In Disturbed Semi-Arid Eucalypt Woodlands. Part 1. Field Data Analysis", *Journal of Environmental Management,* Vol. 23, 1986, pp. 19-33.
28. Karunatillake, S., Squyres, S.W., Taylor, G.J. and 12 others, "Composition of Northern Low-Albedo Regions of Mars: Insights From the Mars Odyssey Gamma Ray Spectrometer", *Journal of Geophysical Research (Planets)*, Vol. 111, 2006, E03S05.
29. Karunatillake, S., McLennan, S., Herkenhoff, K.E., "Regional and Grain Size Influences On the Geochemistry of Soil At Gusev crater, Mars", *Journal of Geophysical Research,* Vol. 115, 2010, E00F04.
30. Kieffer, H.H., Chase, S.C, Miner, E., et al., "Preliminary Report On Infrared Radiometric Measurements From The Mariner 9 Spacecraft", *Journal of Geophysical Research*, Vol. 78, 1973, pp. 4291-4312.
31. Kloer, B.R., "Hybrid Parametric/Non-Parametric Image Classification", *ASPRS/ACSM Annual Convention*, 1994, pp. 307-316.
32. Mellon, M.T., Jakosky, B.M., "Geographic Variations in the Thermal and Diffusive Stability of Ground Ice on Mars", *Journal of Geophysical Research*, Vol. 98, 1993, pp. 3345-3364.
33. Mellon, M.T., Jakosky, B.M., Kieffer, H.H., Christensen P.R., "High-Resolution Thermal Inertia Mapping from the Mars Global Surveyor Thermal Emission Spectrometer", *Icarus*, Vol. 148, 2000, pp. 437-455.
34. Mellon, M.T., Phillips, R.J., "Recent Gullies On Mars and The Source of Liquid Water", Journal of Geophysical Research, Vol. 106, 2001, pp. 1-15.
35. Mellon, M.T., Feldman, W.C., Prettyman, T.H., "The Presence and Stability of Ground Ice In The Southern Hemisphere of Mars", *Icarus*, Vol. 169, 2004, pp. 324-340.
36. Miller, J.D., Yool, S.R., "Mapping Forest Post-Fire Canopy Consumption In Several Overstory Types Using Multi-temporal Landsat TM and ETM data", *Remote Sensing of Environment*, Vol. 82, 2002, pp. 481-496.
37. Milligan, G.W., Cooper, M.C., "An Examination of Procedures For Determining The Number of Clusters In A Data Set.", *Psychometrika*, Vol. 50, 1985, pp. 159-179.
38. Murray, A.T., Estivill-Castro, V., "Cluster Discovery Techniques For Exploratory Spatial Data Analysis", *International Journal of Geographical Information Science*, Vol. 12, 1998, pp. 431-443.
39. Murphy, N., Jakosky, B.M., Mellon, M.T., Budd, D., "Thermophysical Properties of Martian Duricrust Analogs.", *40th Lunar and Planetary Sciences Conference,* Vol. 40, 2009, abstract #1420.
40. Murthy, C.S., Raju,, P.V., Badrinath, K.V., "Classification of Wheat Crop With Multi-temporal Images: Performance of Maximum Likelihood and Artificial Neural Networks", *International Journal of Remote Sensing*, Vol. 24, 2003, pp. 4871-4890.
41. Neugebauer, G., Munch, G., Kieffer, H., et al., "Mariner 1969 Infrared Radiometer Results: Temperatures and Thermal Properties of the Martian Surface", *Astronomical Journal,* Vol. 76, 1971, pp. 719-749.

42. Palluconi, F.D., Kieffer, H.H., "Thermal Inertia Mapping of Mars From 60°S to 60°N", *Icarus*, Vol. 45, 1981, pp. 415-426.
43. Piqueux, S., Christensen, P.R., "A Model of Thermal Conductivity For Planetary Soils: 2. Theory For Cemented Soils", *Journal of Geophysical Research*, Vol. 114, 2009, E09006.
44. Putzig, N.E, Mellon, M.T., Kretke, K.A., Arvidson, R.E., "Global Thermal Inertia and Surface Properties of Mars From The MGS Mapping Mission", *Icarus*, Vol. 173, 2005, pp325-341.
45. Putzig, N.E., "Thermal Inertia and Surface Heterogeneity On Mars", *PhD Dissertation*, 2006.
46. Putzig, N.E. & Mellon, M.T., "Thermal Behaviour of Horizontally Mixed Surfaces On Mars", *Icarus*, Vol. 191, 2007a, pp. 52-67.
47. Putzig, N.E, Mellon, M.T., "Apparent Thermal Inertia and The Surface Heterogeneity of Mars", *Icarus*, Vol. 191, 2007b, pp. 68-94.
48. Richards, J.A., "Remote Sensing Digital Image Analysis – An Introduction", *Springer-Verlag*, Berlin, 1986, pp. 175-204.
49. Rogers, D.A., Bandfield, J.L., Christensen, P.R., "Global Spectral Classification of Martian Low-Albedo Regions With Mars Global Surveyor Thermal Emission Spectrometer (MGS-TES) Data", *Journal of Geophysical Research (Planets)*, Vol. 112, 2007, E02004.
50. Ruff, S.W., Christensen,P.R., "Bright and Dark Regions of Mars: Particle Size and Mineralogical Characteristics Based On The Thermal Emission Spectrometer", *Journal of Geophysical Research*, Vol. 107, 2002, E001580.
51. Sader, S.S., Ahl, D., Liou, W.S., "Accuracy of Landsat-TM and GIS Rule-Based Methods For Forest Wetland Classification", *Remote Sensing of Environment*, Vol. 53, 1995, pp. 133-144.
52. Shkuratov, Y., Starukhina, L., Hoffman, H., Arnold, G., "A Model of Spectral Albedo of Particulate Surfaces: Implications For Optical Properties of The Moon", *Icarus*, Vol. 137, 1999, pp. 235-246.
53. Sizemore, H.G., Mellon, M.T., "Effects of Soil Heterogeneity On Martian Ground-Ice Stability and Orbital Estimates of Ice Table Depth", *Icarus*, Vol. 185, 2006, pp. 358-369.
54. Skinner, J.A., Jr., Hare, T.M., Tanaka, K.L., "Digital Renovation of the Atlas of Mars 1:15,000,000-Scale Global Geologic Series Maps", Lunar and Planetary Sciences Conference, Vol. 38, 2006, abstract #2331.
55. Smith, M.D., Conrath, B.J., Pearl, J.C., Christensen, P.R., "Thermal Emission Spectrometer Observations of Martian Planet-Encircling Dust Storm 2001A", *Icarus*, Vol. 157, 2002, pp. 259-263.
56. Smith, M.D., "Interannual Variability in TES Atmospheric Observations of Mars During 1999-2003", *Icarus*, Vol. 167, 2004, pp. 148-165.
57. Stepinski, T., Vilalta, R., "Digital Topography Models For Martian Surfaces", *IEEE Geoscience and Remote Sensing Letters*, Vol. 2, 2005, pp. 260-264.
58. Stepinski, T.F., Bagaria, C., "Segmentation-Based Unsupervised Terrain Classification For Generation of Physiographic Maps", *IEEE Geoscience and Remote Sensing Letters*, Vol. 6, 2009a, pp. 733-737.
59. Stepinski, T.F., Mendenhall, M.P., Bue, B.D., "Machine Cataloging of Impact Craters On Mars", *Icarus*, Vol. 203, 2009b, pp. 77-87.
60. Swain, P.H., Davis, S.M., "Remote Sensing: The Quantitative Approach", *McGraw-Hill International*, Sheffield, UK, 1978.
61. Swain, P.H., "Pattern Recognition: A Basis For Remote Sensing Data Analysis", LARS information note #111572, Purdue University, 1973.
62. Tamppari, L.K., Smith, M.D., Bass, D.S., Hale, A.S., "Water-Ice Clouds and Dust In The North Polar Region of Mars Using MGS TES Data", *Planetary and Space Science*, Vol. 56, 2008, pp. 227-245.
63. Tanaka, K.L, Skinner, J.A., Hare, T.M., "Geologic Map of the Northern Plains of Mars", US Geological Survey, Scientific Investigations Map 2888, 2005.
64. Titus, T.N., Kieffer, H.H., Christensen, P.R., "Exposed Water Ice Discovered Near The South Pole of Mars", *Science*, Vol. 299, 2003, pp. 1048-1051.
65. Tou, J.T., Gonzalez, R.C., 'Pattern Recognition Principes', *Adisson Wesley*, London, 1974.
66. Turcotte, D.L., Scherbakov, R., Malamund, B.D., Kucinskas, A.B., "Is the Martian Crust Also The Martian Elastic Lithosphere?", *Journal of Geophysical Research*, Vol. 107, 2002, E001594.
67. Wackerly, D.D., Mendenhall III, W., Scheaffer, R.L. "Mathematic Statistics With Applications (6th ed.)" *Thomson Learning*, Pacific Grove, 2002.

68. Walker, J., Jupp, D., Penridge, L., Tian, G., "Interpretation of Vegetation Structure In Landsat MSS Imagery: A Case Study In Disturbed Semi-Arid Eucalypt Woodlands. Part I: Field Data Analysis.", *Journal of Environmental Management*, Vol. 23, 1986, pp 19-33.
69. Wang, K., Wang, P., Liu, J., Sparrow, M., Haginoya, S., Zhou, X., 'Variation of Surface Albedo and Soil Thermal Parameters With Soil Moisture Content At A Semi-Desert Site On The Western Tibetan Plateau.', *Boundary-Layer Meteorology*, Vol. 116, 2005, pp. 117-129.
70. Wilson, R.J., Neumann, G.A., Smith, M.D., "Diurnal Variation and Radiative Influence of Martian Water Ice Clouds", *Geophysical Research Letters*, Vol. 34, 2007, L02710.